Preliminary measurement of $R_{\rm s}$=$\Gamma_{\rm s\bar{s}}/\Gamma_{had}$ using the DELPHI detector at LEP 100

K. Karafasoulis, A. Markou
NCSR Demokritos, Athens
M. Dracos
IReS/ULP, Strasbourg
E. Katsoufis
NTU, Athens

Abstract

A measurement of the branching fraction $R_{\rm s}$=$\Gamma_{\rm s\bar{s}}/\Gamma_{had}$ of the $\rm Z^0$ into strange quarks was made. For this measurement energetic ϕ^0 mesons decaying into K^+K^- and charged kaons were used to tag the presence of $e^+e^- \rightarrow Z^0 \rightarrow s\bar{s}$ events. 1.4 million hadronic $\rm Z^0$ events collected by the DELPHI detector in 1994 have been used for this measurement. The Ring Imaging Cherenkov detector (RICH) was used to identify the charged kaons. For ϕ^0's with a fraction of momentum higher than 0.5 a $\rm s\bar{s}$ event purity of 77% was reached while for charged kaon analysis this purity was at the level of 40%. The ratio $R_{\rm s}$ was measured to be:

$$R_s = 0.233 \pm 0.003(stat.) \pm 0.024(syst.)$$

in agreement with the Standard Model value and the already measured value of $R_{\rm b}$.

1 Introduction

The Standard Model predicts that the partial decay width $\Gamma_{Z^0 \to q\bar{q}}$ in the Born approximation is given by:

$$\Gamma_{Z^0 \to q\bar{q}} = \frac{G_F M_Z^3}{8\pi\sqrt{2}} \sqrt{1-4\mu^q} \left[(g_V^q)^2 \cdot (1+2\mu^q) + (g_A^q)^2 \cdot (1-4\mu^q) \right]$$

where $\mu^q = (m^q)^2/M_Z^2$, m^q the mass of quark q, $g_A^q = I_3^q$ the axial vector coupling for quark q and $g_V^q = I_3^q - 2Q_q \sin^2\vartheta_w$, the vector coupling .

In the Born approximation when the quark masses are neglected, the fraction of $q\bar{q}$ events in the Z^0 hadronic decays, R_{q}, is:

$$R_q = \frac{\Gamma_{q\bar{q}}}{\Gamma_{had}} = \frac{(g_A^q)^2 + (g_V^q)^2}{\sum\limits_{q'} (g_A^{q'})^2 + (g_V^{q'})^2} \tag{1}$$

The Standard Model predicts for R_{q} the values given by table 1 [1]. The difference between R_{s} and R_{b} is mainly due to the top quark coupling.

Table 1: *R_{q} values predicted by the Standard Model and measured experimentally.*

R_q	S.M.	exp. values
R_d	0.2198	
R_u	0.1724	0.160 ± 0.027
R_s	0.2198	
R_c	0.1723	0.1734 ± 0.0048
R_b	0.2157	0.2170 ± 0.0009

The values of R_{c} and R_{b} have already been measured at LEP and SLD [2]. The world average for these values is also given by table 1. The experimental value for R_{u} is given by OPAL Collaboration [3]. Comparing the measured values of R_{b} and R_{s} the universality of the $d-$like quark couplings predicted by the Standard Model of electroweak interactions can be tested.

In contrast with the $\mathrm{b\bar{b}}$ and $\mathrm{c\bar{c}}$ events where secondary vertices, large track impact parameters and the presence of leptons and high momentum B and D mesons can be used for flavour tagging [4], $\mathrm{s\bar{s}}$ events are more difficult to recognize. The DELPHI experiment with its RICH detector has a unique capability to identify charged kaons up to 20 GeV/c providing a way to tag particles which could contain the primary $s-$quark. This advantage has already been used to measure the $s-$quark forward–backward asymmetry at the Z^0 peak using energetic charged kaons [5]. This was the first test of the universality of the coupling constants between $s-$ and $b-$quarks.

In this paper, energetic ϕ^0's decaying into K^+K^- and charged kaons are used to tag $e^+e^- \to Z^0 \to s\bar{s}$ events. These energetic mesons have a high probability to contain the primary $s-$quark. Fig. 1 and 2 show the composition of selected events as a function of the low limit cut on the fraction of momentum for ϕ^0's and charged kaons respectively, as predicted by JETSET PS 7.3 [6].

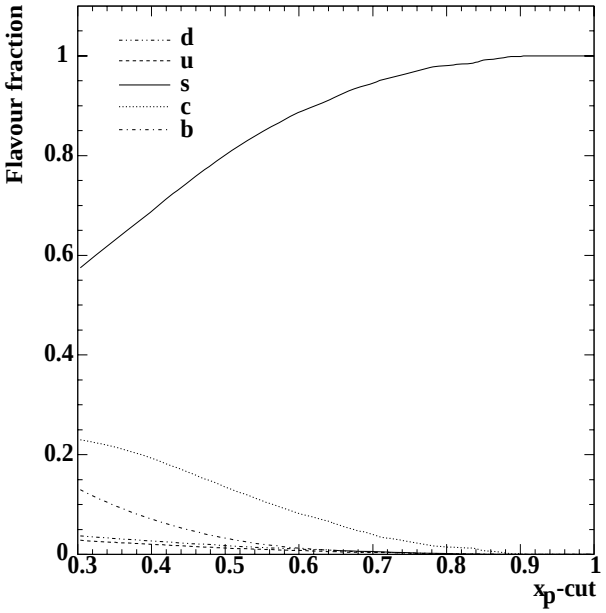

Figure 1: *Flavour event composition versus* $x_p - cut$ *of* ϕ^0.

For $x_p - cut = 0.4$, a $s\bar{s}$ event purity of 69% can be reached for ϕ^0's. For kaons and for $x_p - cut = 0.20$ (cut used in this analysis), a $s\bar{s}$ event purity of 43% is expected. In this last case the systematic errors are expected to be higher than for the case where ϕ^0's are used, but this could be compensated by the low statistical error due to the big number of charged kaons. The main contamination for both cases come from $c\bar{c}$ events.

2 The Detector

A detailed description of the DELPHI detector and performance can be found elsewhere [7]. Only a brief description of the components used in this analysis is given here.

The Vertex Detector (VD) consists of 3 cylindrical layers of silicon, at radii 6.3 cm, 9.0 cm and 10.9 cm respectively and a common length of 24 cm. Its aim is to measure $R\phi$ coordinates accurately. Since 1994, the 6.3 cm and 10.9 cm layers have been updated to give also Rz information. The VD covers the polar angle domain between 25° and 155° (inner layer).

The Inner Detector (ID), a cylindrical drift chamber, provides trigger and vertex information. The polar angle coverage of the ID is from 23° to 157°.

The Time Projection Chamber (TPC), the main tracking device of DELPHI, is a cylinder of 30 cm inner radius and 122 cm outer radius with a length of 2.7 m. It provides a three dimensional track information of charged particles in the barrel region.

The Outer Detector (OD), consists of 5 layers of drift cells at a radius between 197 cm and 206 cm, covering polar angles between 42° and 138°. It is used for fast triggering and momentum reconstruction.

The Barrel RICH, covering a cylindrical area with a polar angle between 40° and

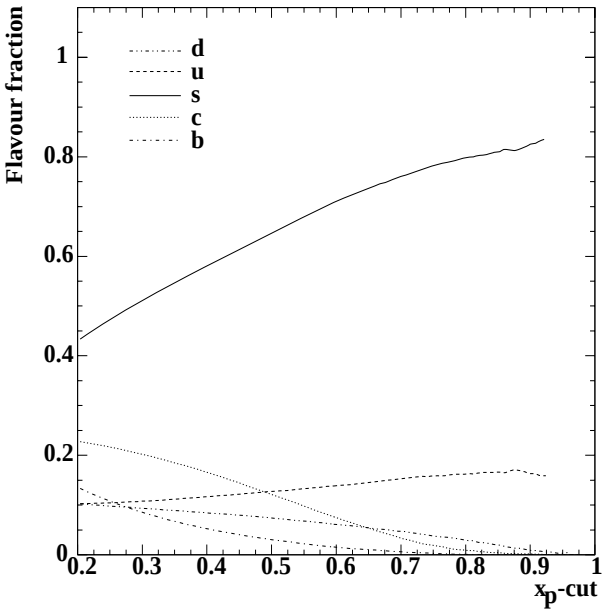

Figure 2: *Flavour event composition versus x_p − cut of charged kaons.*

140°, identifies the charged particles by measuring the emission angle of the Cherenkov radiation and thus its velocity. Combining the velocity information and the momentum measurement provided by the tracking devices, the mass of the charged particles is extracted. Two different radiators are used in the Barrel RICH, one liquid (C_6F_{14}) and one gaseous (C_5F_{12}) to cover a large momentum range in $K^{\pm}/\pi^{\pm}$ separation from 0.8 GeV/c to 20 GeV/c.

3 Selection Criteria

The data used in this analysis have been collected by the DELPHI detector at LEP during 1994. The hadronic event selection criteria ($e^+e^- \to Z^0 \to q\bar{q}$) are described in [8]. They select 95% of hadronic events with estimated contamination from $Z \to \tau^+\tau^-$ less than 0.1% and negligible contamination from other processes as beam–gas and two photon events. These selection criteria are not expected to bias the flavour composition of the Z^0 hadronic events. Only extra criteria related to the present analysis are given here.

- Only candidate charged kaons well in the Barrel RICH acceptance were retained ($0.04 <| \cos\theta_K |< 0.68$).
- Only candidate charged kaons crossing the Barrel RICH drift tubes not presenting hardware problems (chamber trips, too many dead electronic channels) were accepted. Less than 1% of the considered tracks were suffering by the above problems.

4 Method

In this section the way of extracting the ratio $R_{\rm s}$ from the measured numbers of ϕ^0's (N^{ϕ^0}) and charged kaons (N^K), is explained.

The probability per hadronic event that one of the above particles is produced in all $\rm Z^0$ hadronic events is:

$$\frac{N^\lambda}{N_{had}} = \sum_q \frac{N(q\bar{q}\to\lambda)}{N(Z\to hadrons)} = \sum_q \frac{N(q\bar{q}\to\lambda)}{N_{\rm q\bar{q}}} \times \frac{N_{\rm q\bar{q}}}{N(Z\to hadrons)} \tag{2}$$

where N_λ/N_{had} is the reconstructed number of λ's per hadronic event with λ being $\phi^0 \to K^+K^-$ or $K^\pm$ and $N_{\rm q\bar{q}}$ the number of observed events from flavour $q = (d,\ u,\ s,\ c,\ b)$. By putting $R_q = N_{\rm q\bar{q}}/N_{had}$, equation (2) leads to:

$$\frac{N^\lambda}{N_{had}} = \sum_q \alpha_q^\lambda \cdot R_q \tag{3}$$

where, finally, α_q^λ is the probability to observe (or reconstruct) particle λ produced by flavour q ($Z^0 \to q\bar{q} \to \lambda + X$).

$$R_s = \frac{1}{\alpha_s^\lambda}\left[\frac{N^\lambda}{N_{had}} - \sum_{q\neq s} \alpha_q^\lambda \cdot R_q\right] \tag{4}$$

The coefficients α_q^λ are estimated from full Monte Carlo simulation (DELSIM [9]) as a function of the transferred momentum of the reconstructed particle $x_p = p/E_{beam}$ (where $E_{beam} = 45.625$ GeV the beam energy). From this formula one can see the importance of having α_s^λ as high as possible (high $s-$purity) keeping $\alpha_{q\neq s}^\lambda$ low (to limit contamination from other flavours).

5 Analysis

For kaon identification for ϕ^0 reconstruction, the maximum likelihood method RINGSCAN [10] was used. For the measurement of N^{ϕ^0}, the K^+K^- invariant mass (m_{KK}) distribution was reconstructed. Charged tracks were accepted as candidates to form a ϕ^0 vertex if their momentum was 1 GeV/c< $p_{K^\pm}$ <20 GeV/c in order the RICH to be able to identify them.

As can be seen by fig. 3a-7a (m_{KK} distribution), the contribution of the combinatorial background makes necessary the identification of the charged tracks with the RICH detector in order to improve the ratio signal to background.

For charged kaon analysis, in order the charged tracks to be identified by the RICH (imposing the kaon momentum upper limit) and to keep a reasonable $\rm s\bar{s}$ event purity (imposing the kaon momentum lower limit), only tracks with a momentum between 10 GeV/c and 20 GeV/c were used. In this case, for charged kaon identification, the RNEWTAG [11] method based on a clustering algorithm, was used. To select well reconstructed tracks and limit pion contamination, the tracks are required to have TPC (tracking detector before the Barrel RICH) and OD (tracking detector after the Barrel RICH) information. This requirement has caused a 35% track loss.

5.1 ϕ^0 Analysis

The fraction of momentum x_p carried by ϕ^0's was split into the five ranges given by Table 2 in a way to have enough statistics in each range.

Table 2: *x_p ranges for the ϕ^0 analysis.*

	x_p range
1	$0.390 < x_p < 0.455$
2	$0.455 < x_p < 0.500$
3	$0.500 < x_p < 0.585$
4	$0.585 < x_p < 0.694$
5	$0.694 < x_p$

For each of the above ranges the invariant mass m_{KK} distribution was reconstructed with one or both tracks identified as kaons. The invariant mass distribution was fitted with the function:

$$\frac{dN}{dm} = \alpha_1 \cdot BW + \alpha_2 \cdot BG$$

where BW is a Breit–Wigner distribution describing the ϕ^0 signal and BG is the function used to fit the background. As the track resolution and, therefore, the width of the ϕ^0 signal depend on the track momentum, the x_p ranges must not be too large in order to well fit the signal by a simple Breit–Wigner distribution. Several background parametrization functions were used. The best fit (best χ^2/d.o.f) was obtained by smoothing the shape of the background as it was taken from the full Monte Carlo simulation DELSIM for each x_p range. In this case, the only free parameter for BG was the normalization factor.

The total number (N^{ϕ^0}) of ϕ^0 mesons and the average kaon identification efficiency $\epsilon_{K^\pm}$ per x_p range, were calculated from the real data for the process $\phi^0 \to K^+K^-$, comparing the number of ϕ^0's ($N^{\phi^0}_{or}$) obtained when one of the two kaons was identified with those ($N^{\phi^0}_{and}$) obtained when both kaons were identified (fig. 3a-7a, ii and iii) using the expressions:

$$N^{\phi^0}_{or} = (1 - (1 - \epsilon_{K^\pm})^2) \cdot N^{\phi^0} \tag{5}$$

and:

$$N^{\phi^0}_{and} = \epsilon^2_{K^\pm} \cdot N^{\phi^0} \tag{6}$$

Using equations (5) and (6), the kaon identification efficiency and the number of ϕ^0's before kaon identification are given by:

$$N^{\phi^0} = \frac{(N^{\phi^0}_{or} + N^{\phi^0}_{and})^2}{4N^{\phi^0}_{and}} \tag{7}$$

and:

$$\epsilon_{K^\pm} = \frac{2N_{and}^{\phi^0}/N_{or}^{\phi^0}}{1 + N_{and}^{\phi^0}/N_{or}^{\phi^0}} \tag{8}$$

For this method, the assumption that the identification probabilities of the two kaons were uncorrelated has been done. Although the angle between the two kaons coming from a ϕ^0 decay is small (see section 5.1.1), the distance between the two tracks when they cross the Barrel RICH is large enough (mainly due to the magnetic field) to avoid significant disturbance of one Cherenkov ring to the other one. The particle identification method used [10] takes implicitly into account non uniform background which could come from neighbouring rings. To justify this assumption, the method described in ref. [12] has been used, i.e, a correlation between the identification probabilities of the two kaons has been searched. As in ref. [12], no significant effect has been observed. In order this eventual correlation to produce a systematic error on $R_{\rm s}$, it must also not be well reproduced by the simulation. As it is discussed in section 5.1.1 (here after), no significant difference is observed between data and simulation concerning particle identification. Problems concerning the track reconstruction (and not the particle identification) coming from the small angle between the two tracks are discussed in section 5.1.1.

Thanks to the detector resolution and to the fact that the ϕ^0 is a narrow resonance, the number of ϕ^0's can also be estimated without particle identification but with a much worse signal to background ratio. As a cross-check of the number of ϕ^0's (N^{ϕ^0}) extracted using kaon identification per x_p range, this number has also been extracted by fitting directly the ϕ^0 number ($N_{noid}^{\phi^0}$) without particle identification. Table 3 gives the obtained numbers and the $\chi^2/d.o.f$ of the corresponding fits. A good agreement is observed between the two set of numbers ($N_{noid}^{\phi^0}$ and N^{ϕ^0}) while the $\chi^2/d.o.f$ values are closed to 1. Fig. 3a-7a (i for $N_{noid}^{\phi^0}$, ii for $N_{or}^{\phi^0}$ and iii for $N_{and}^{\phi^0}$) present also these fits. The majority of the undulations of the fit of the background visible on these figures, is due to other particle reflections (ρ^0, ρ^+, K^{*0}, ω) taken partially into account by the smoothing of the simulated background. Some of them are also due to Monte Carlo statistics and are not significant.

Table 3: *Number of fitted ϕ^0's and corresponding $\chi^2/d.o.f$ for data using loose $K^\pm$ identification.*

N	$0.390 < x_p < 0.455$	$0.455 < x_p < 0.500$	$0.500 < x_p < 0.585$	$0.585 < x_p < 0.694$	$0.694 < x_p$
$N_{noid}^{\phi^0}$	994 ± 106	773 ± 72	961 ± 77	509 ± 66	207 ± 41
$\chi^2(N_{noid}^{\phi^0})$	1.16	1.13	1.11	1.04	1.26
$N_{or}^{\phi^0}$	955 ± 89	619 ± 57	805 ± 62	474 ± 57	206 ± 35
$\chi^2(N_{or}^{\phi^0})$	1.04	0.96	1.28	0.98	1.04
$N_{and}^{\phi^0}$	577 ± 49	342 ± 29	492 ± 36	302 ± 32	157 ± 25
$\chi^2(N_{and}^{\phi^0})$	1.02	1.00	1.28	0.93	0.83
N^{ϕ^0}	1017 ± 126	675 ± 80	855 ± 89	498 ± 80	210 ± 52
ϵ_K	75.3 ± 5.2	71.2 ± 5.0	75.9 ± 4.4	77.8 ± 6.8	86.5 ± 10.4

For particle identification, a loose tag corresponding to about 75% kaon identification efficiency for the whole kaon momentum range, has been used. A second cross-check has been done using a more severe particle identification (standard tag) corresponding to about 60% kaon identification efficiency. The extracted numbers are given by table 4.

These numbers (N^{ϕ^0}) are also in a good agreement with the numbers given by table 3 proving that the obtained numbers were robust.

Table 4: *Number of fitted ϕ^0's and corresponding $\chi^2/d.o.f$ for data using standard $K^{\pm}$ identification.*

N	$0.390 < x_p < 0.455$	$0.455 < x_p < 0.500$	$0.500 < x_p < 0.585$	$0.585 < x_p < 0.694$	$0.694 < x_p$
$N^{\phi^0}_{noid}$	994 ± 106	773 ± 72	961 ± 77	509 ± 66	207 ± 41
$\chi^2(N^{\phi^0}_{all})$	1.16	1.13	1.11	1.04	1.26
$N^{\phi^0}_{or}$	832 ± 76	528 ± 48	684 ± 50	404 ± 44	178 ± 35
$\chi^2(N^{\phi^0}_{or})$	0.91	1.10	1.17	0.79	1.02
$N^{\phi^0}_{and}$	365 ± 34	201 ± 20	349 ± 29	179 ± 22	74 ± 13
$\chi^2(N^{\phi^0}_{and})$	1.08	1.11	1.17	1.07	0.90
N^{ϕ^0}	981 ± 110	661 ± 71	764 ± 75	475 ± 65	215 ± 50
ϵ_K (%)	56.3 ± 4.3	55.1 ± 4.6	67.6 ± 4.2	61.4 ± 5.9	58.7 ± 9.7

5.1.1 Comparison of real and simulated data

The invariant mass distribution for the five x_p ranges were compared with those obtained using real data (fig. 3a-7a). A good agreement in all x_p ranges was observed, except for the last one ($x_p > 0.694$), where the detector dispersion was significantly stronger for the real data (fig. 7(a)) producing a broader ϕ^0 distribution.

For this last x_p range, in order to be sure that the ϕ^0 reconstruction efficiency was well described by the simulated data and that the problem was just a resolution discrepancy created mainly by the small angle between the two tracks, a special study was done. Indeed, overlapping tracks coming from energetic ϕ^0's could cause problems in the track reconstruction. To prove that this fact was not causing ϕ^0 losses not well reproduced by the simulation, the distribution of the angle θ_{KK} between the two candidate kaons giving an invariant mass around the ϕ^0 mass, was compared with the simulated one for all the x_p ranges. Fig. 3b-7b show the comparison between data and Monte Carlo of $\cos\theta_{KK}$ distributions normalized to the number of events. A very good agreement is observed between the two sets of distributions, even for $x_p > 0.694$ (fig. 7b) proving that reconstruction efficiencies in real data were well reproduced in Monte Carlo. The agreement was also kept after particle identification (fig. 3b-7b, ii and iii) proving also that the track resolution problem was not affecting significantly the RICH identification capability.

Finally, the obtained numbers from simulated data corresponding to those (data) of table 3, are given by table 5. A good agreement is also observed between data and Monte Carlo concerning the kaon identification efficiency $\epsilon_{K^{\pm}}$ extracted using equation (8). ϵ_K^{true} is the kaon efficiency obtained using the known $N^{\phi^0}_{or}$ and $N^{\phi^0}_{and}$ numbers from simulated data. A good agreement is also observed between $\epsilon_{K^{\pm}}$ and ϵ_K^{true}.

Table 5: *Number of fitted ϕ^0's and corresponding $\chi^2/d.o.f$ for simulated data using loose $K^{\pm}$ identification.*

N	$0.390 < x_p < 0.455$	$0.455 < x_p < 0.500$	$0.500 < x_p < 0.585$	$0.585 < x_p < 0.694$	$0.694 < x_p$
$N^{\phi^0}_{true}$	1130	616	826	572	230
$N^{\phi^0}_{noid}$	1137 ± 100	632 ± 64	846 ± 69	577 ± 49	203 ± 24
$\chi^2(N^{\phi^0}_{noid})$	1.05	0.84	0.93	0.50	0.84
$N^{\phi^0}_{or}$	1028 ± 80	569 ± 51	801 ± 58	544 ± 42	188 ± 21
$\chi^2(N^{\phi^0}_{or})$	1.13	0.82	0.77	0.48	1.26
$N^{\phi^0}_{and}$	641 ± 46	346 ± 28	515 ± 35	404 ± 30	134 ± 16
$\chi^2(N^{\phi^0}_{and})$	1.05	0.84	0.99	0.63	1.02
N^{ϕ^0}	1086 ± 114	605 ± 72	841 ± 84	556 ± 63	193 ± 33
ϵ_K (%)	76.8 ± 4.4	75.6 ± 5.0	78.2 ± 4.2	85.2 ± 4.7	83.2 ± 7.0
ϵ_K^{true} (%)	73.8	75.4	77.3	81.6	82.1

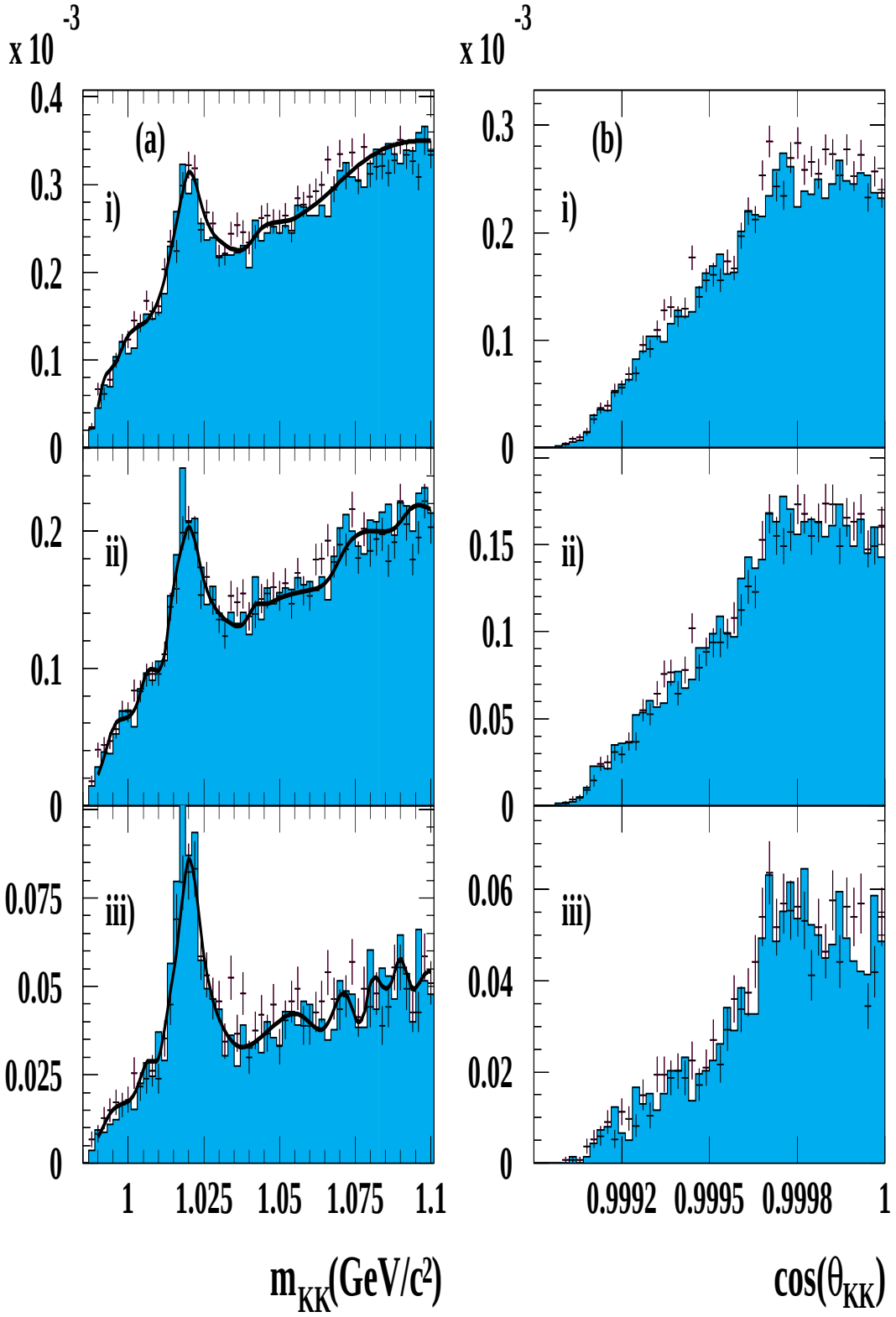

Figure 3: *Invariant mass m_{KK} and $\cos\theta_{KK}$ distributions for real and simulated data for 0.390< x_p <0.455, i) without identification, ii) when one of the two kaons is identified and iii) when both kaons are identified (the distributions are normalized to the number of events).*

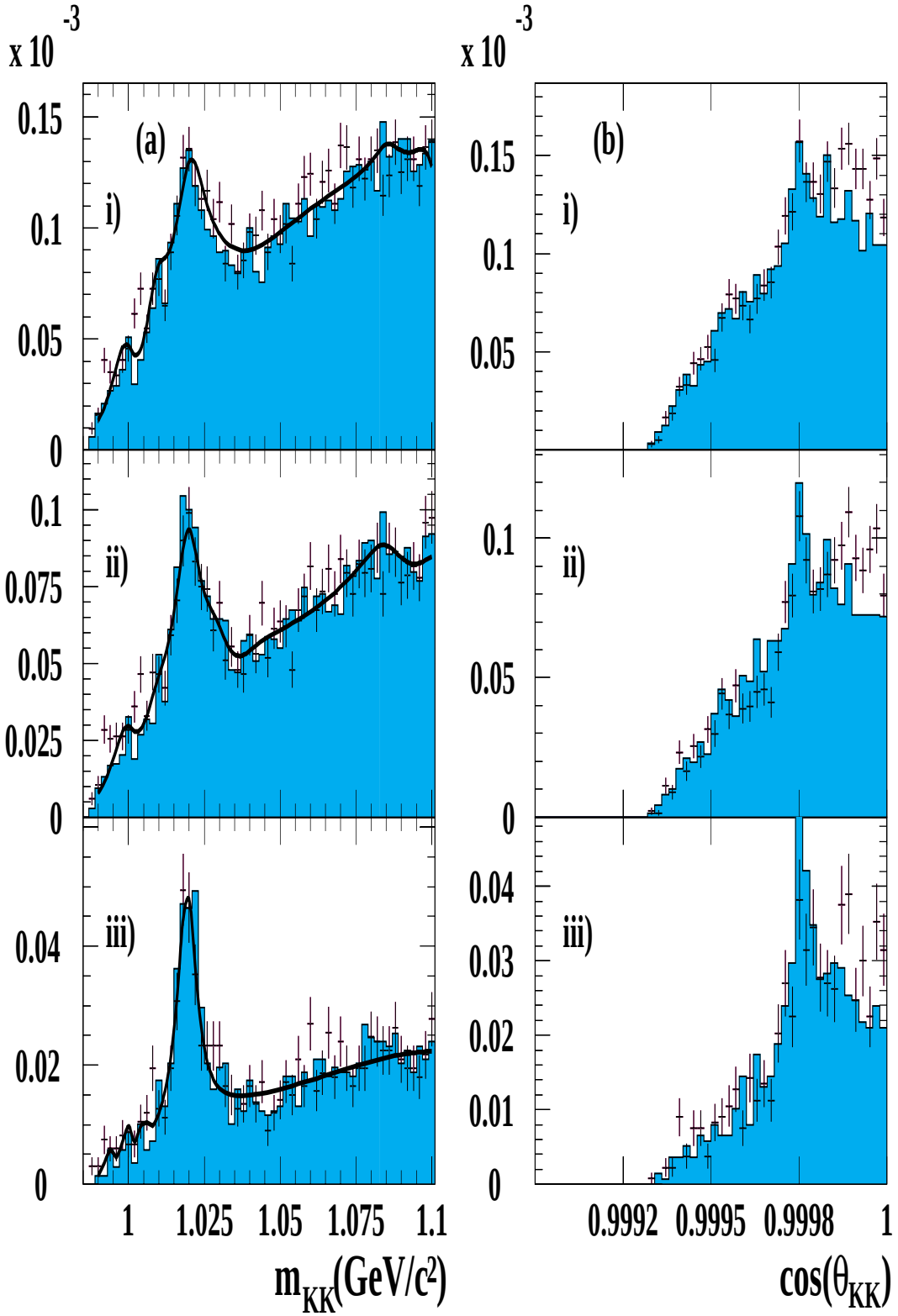

Figure 4: *Invariant mass m_{KK} and $\cos\theta_{KK}$ distributions for real and simulated data for 0.455< x_p <0.500, i) without identification, ii) when one of the two kaons is identified and iii) when both kaons are identified (the distributions are normalized to the number of events).*

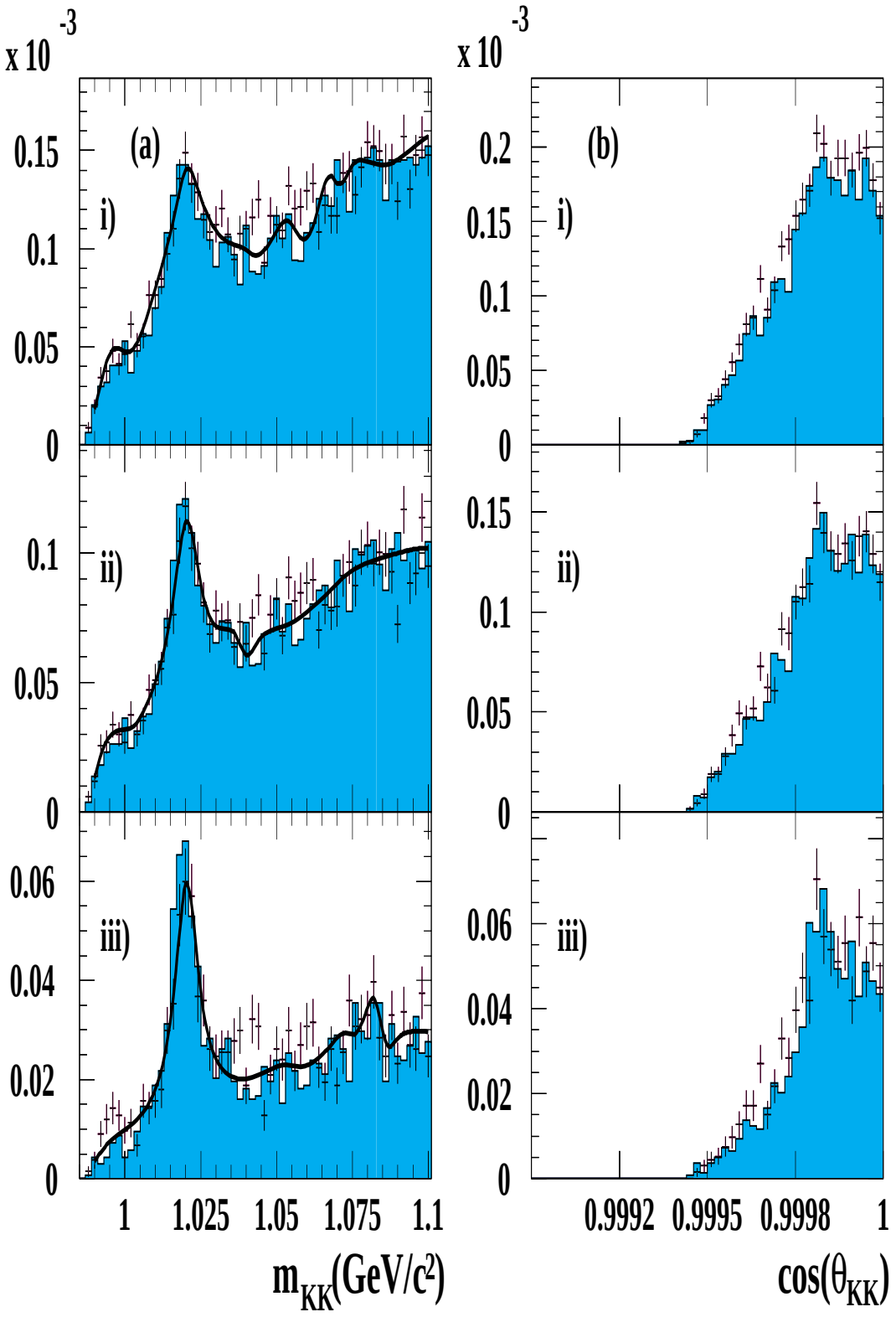

Figure 5: *Invariant mass m_{KK} and $\cos\theta_{KK}$ distributions for real and simulated data for 0.500< x_p <0.585, i) without identification, ii) when one of the two kaons is identified and iii) when both kaons are identified (the distributions are normalized to the number of events).*

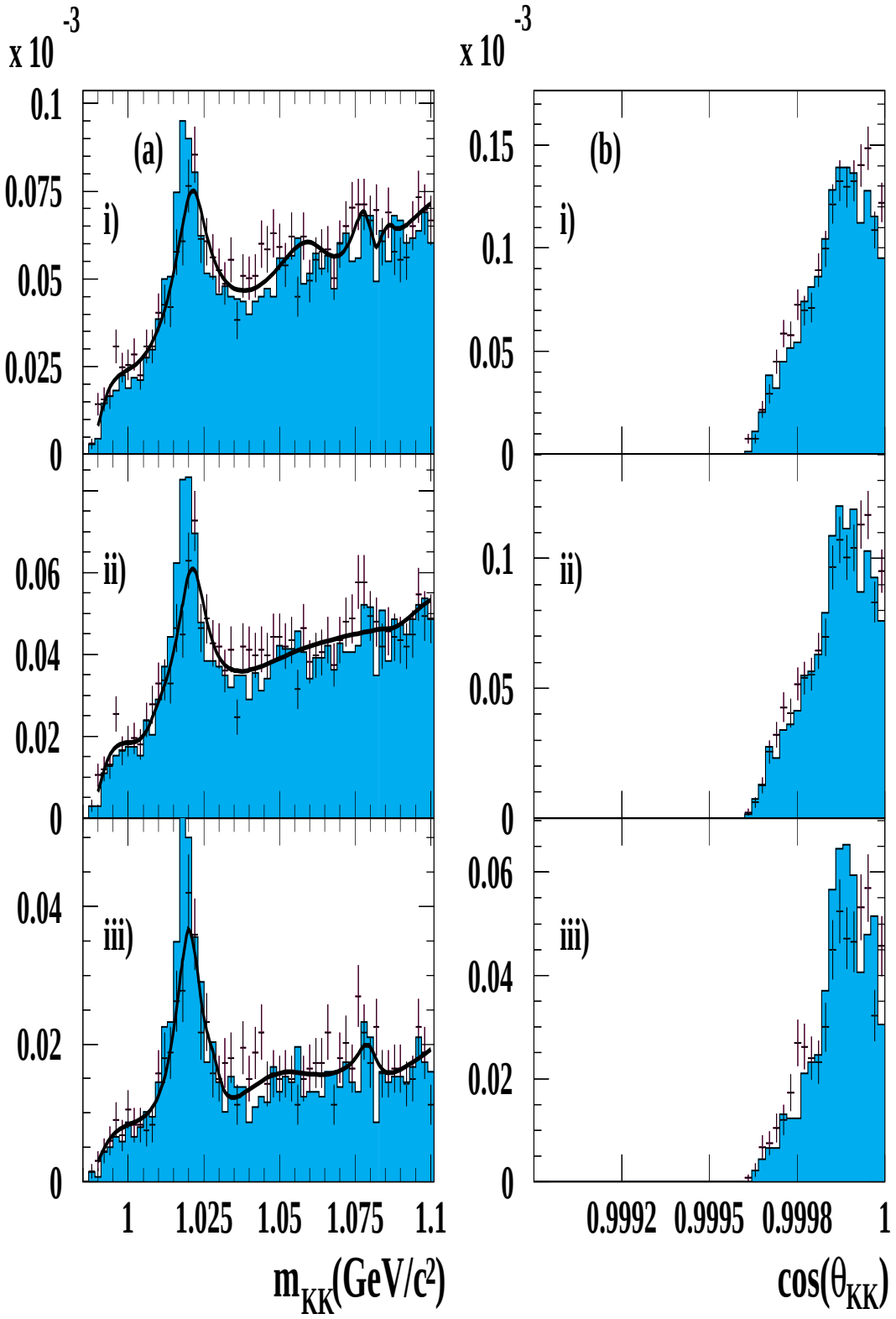

Figure 6: *Invariant mass m_{KK} and $\cos\theta_{KK}$ distributions for real and simulated data for 0.585< x_p <0.694, i) without identification, ii) when one of the two kaons is identified and iii) when both kaons are identified (the distributions are normalized to the number of events).*

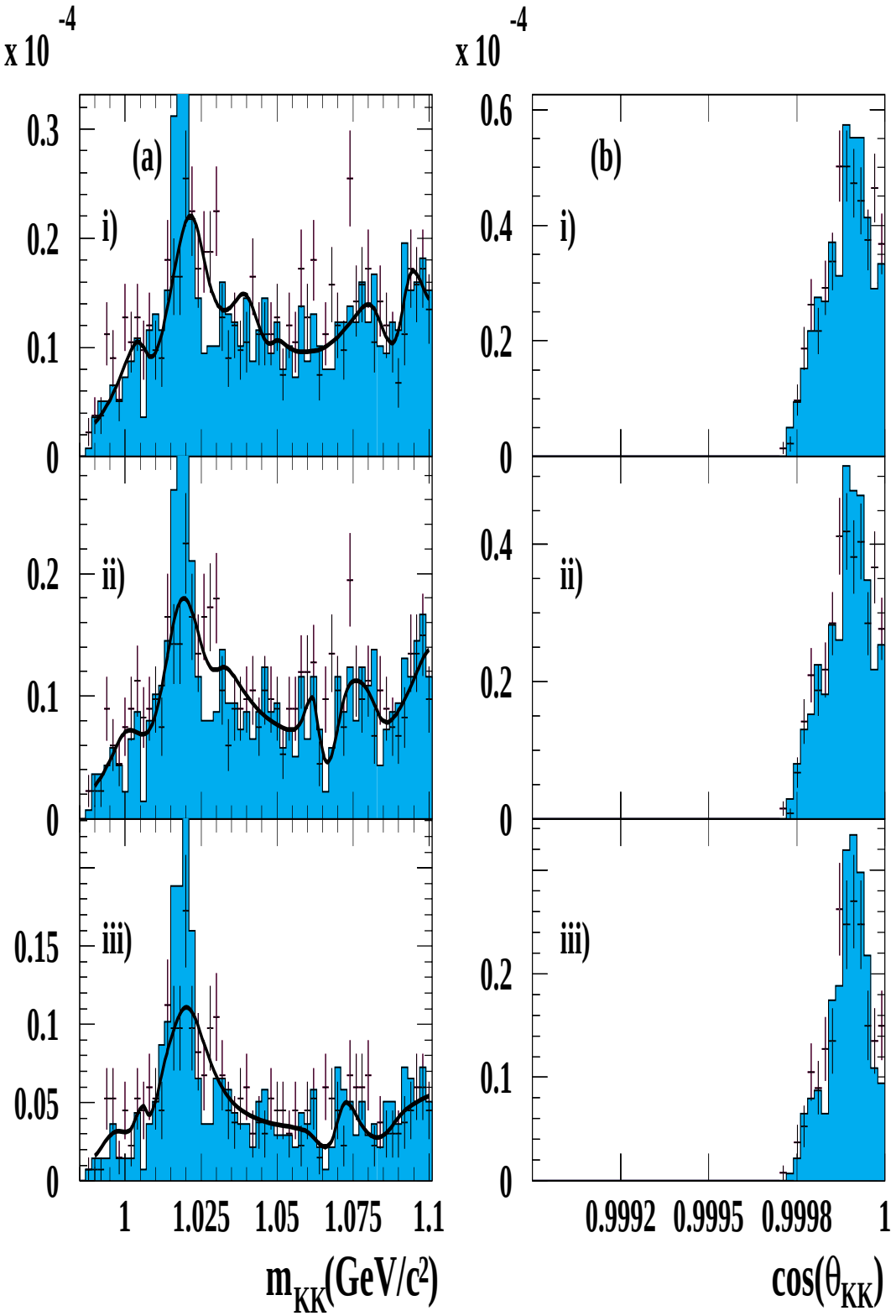

Figure 7: *Invariant mass m_{KK} and $\cos\theta_{KK}$ distributions for real and simulated data for x_p >0.694, i) without identification, ii) when one of the two kaons is identified and iii) when both kaons are identified (the distributions are normalized to the number of events).*

5.1.2 R_s using ϕ^0's

Given N^{ϕ^0}, in order to calculate R_s, the coefficients $\alpha_q^{\phi^0}$ of the equation (4) are needed. These numbers have been extracted using full simulation knowing the flavour from which the reconstructed ϕ^0's have been initiated. Table 6 gives the $\alpha_q^{\phi^0}$ values per $x_p - cut$. The numbers of reconstructed ϕ^0's per x_p range and per hadronic event used for R_s calculation are given by table 7.

Table 6: $\alpha_q^{\phi^0}$ *coefficients as calculated from full simulation per flavour for* ϕ^0 *analysis.*

flavour	$x_p > 0.390$	$x_p > 0.450$	$x_p > 0.500$	$x_p > 0.585$	$x_p > 0.694$
d	$3.55\text{x}10^{-4}$	$1.87\text{x}10^{-4}$	$1.08\text{x}10^{-4}$	$3.61\text{x}10^{-5}$	$6.57\text{x}10^{-6}$
u	$3.71\text{x}10^{-4}$	$1.90\text{x}10^{-4}$	$1.26\text{x}10^{-4}$	$5.90\text{x}10^{-5}$	$2.53\text{x}10^{-5}$
s	$7.36\text{x}10^{-3}$	$5.32\text{x}10^{-3}$	$4.10\text{x}10^{-3}$	$2.23\text{x}10^{-3}$	$6.69\text{x}10^{-4}$
c	$2.86\text{x}10^{-3}$	$1.67\text{x}10^{-3}$	$1.07\text{x}10^{-3}$	$3.43\text{x}10^{-4}$	$7.62\text{x}10^{-5}$
b	$9.02\text{x}10^{-4}$	$4.49\text{x}10^{-4}$	$2.41\text{x}10^{-4}$	$6.37\text{x}10^{-5}$	$3.35\text{x}10^{-6}$

Table 7: N^{ϕ^0} *per hadronic event and reconstruction efficiency* (ϵ_{rec}) *of* ϕ^0*'s (not including particle identification) versus* x_p *range.*

x_p interval	N^{ϕ^0}/event $\pm$ stat. error ($\times 10^{-4}$)	ϵ_{rec}
$0.390 < x_p < 0.455$	7.74 ± 0.99	40.3%
$0.455 < x_p < 0.500$	4.73 ± 0.64	42.7%
$0.500 < x_p < 0.585$	6.41 ± 0.72	42.5%
$0.585 < x_p < 0.694$	3.63 ± 0.62	36.7%
$0.694 < x_p$	1.63 ± 0.43	17.6%

Table 8: *Flavour composition of selected events for* ϕ^0 *analysis.*

flavour	$x_p > 0.390$	$x_p > 0.450$	$x_p > 0.500$	$x_p > 0.585$	$x_p > 0.694$
d	3.2%	2.5%	2.0%	1.4%	0.1%
u	2.6%	2.0%	1.8%	1.6%	2.3%
s	66.2%	72.0%	76.5%	85.1%	90.3%
c	20.0%	17.6%	15.4%	9.7%	6.5%
b	7.9%	6.0%	4.4%	2.2%	0.0%

Reconstruction losses, mainly at high x_p, have the tendency to distort the flavour composition of the selected events given by fig. 2 (JETSET). Table 7 gives the reconstruction efficiency per x_p range, (not including losses due to particle identification) while fig. 8 and table 8 present the flavour composition for reconstructed ϕ^0's for each $x_p - cut$. For x_p greater than 0.39 the $s\bar{s}$ purity goes from 69% (fig. 1) down to 66% (fig. 8). Three

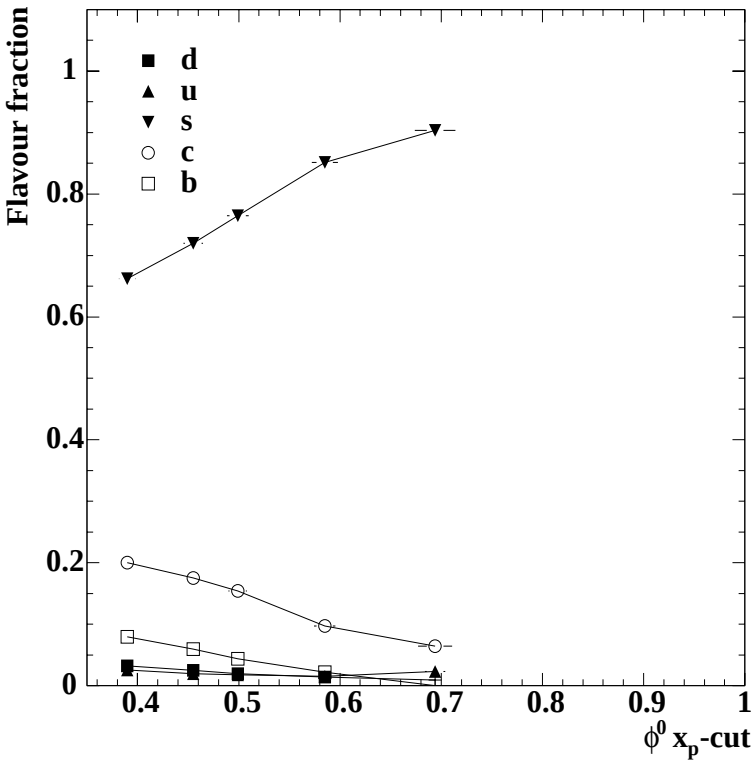

Figure 8: *Flavour event composition versus $x_p - cut$ of reconstructed ϕ^0's.*

approaches have been used to calculate the ratio $R_{\rm s}$ based on the formulas presented the section 4:

1. $R_{\rm s}$ is calculated from equation (4) assuming that:

$$R_{\rm d} = R'_{\rm b} \quad \Delta R_{\rm d} = 3\Delta R_{\rm b}$$
$$R_{\rm u} = R_{\rm c} \quad \Delta R_{\rm u} = 3\Delta R_{\rm c}$$

where $R'_{\rm b}$ is equal to $R_{\rm b}$ increased by 1.9%, the amount by which the measured value of $R_{\rm b}$ is expected to be smaller than $R_{\rm d}$ due to vacuum polarization corrections depending on the $t-$quark mass [2]. $R_{\rm c}$ is also the measured value (table 1). The obtained result is:

$$R_s = 0.218 \pm 0.020 \ (stat.) \tag{9}$$

To check the stability of the result versus the x_p-cut (and consequently the $s-$quark purity), $R_{\rm s}$ has also been calculated for $x_p > 0.455$ ($\rm s\bar{s}$ purity=72%) and $x_p > 0.500$ ($\rm s\bar{s}$ purity=77%). The following values have been extracted:

$$R_s = 0.228 \pm 0.022 \ (stat.) \ (x_p > 0.455)$$
$$R_s = 0.217 \pm 0.024 \ (stat.) \ (x_p > 0.500)$$

consistent with the previous value (9) (the systematic uncertainties are discussed in next section). On top of that, if for $R_{\rm u}$ and $\Delta R_{\rm u}$ values, the results of OPAL [3] (table 1) are taken, the previous results become:

$$\begin{aligned} R_s &= 0.218 \pm 0.020\ (stat.)\ (x_p > 0.390) \\ R_s &= 0.229 \pm 0.022\ (stat.)\ (x_p > 0.455) \\ R_s &= 0.217 \pm 0.024\ (stat.)\ (x_p > 0.500) \end{aligned}$$

The results are not very sensitive to $\Delta R_{\rm u}$ because of the low contamination coming from u$\bar{\rm u}$ events (table 8).

2. $R_{\rm b}$, $R_{\rm c}$ and $R_{\rm u}$ are considered to be the measured values. If one considers that:

$$\sum_q R_{\rm q} = 1 \tag{10}$$

$R_{\rm d}$ is given by: $R_{\rm d} = 1 - R_{\rm s} - (R_{\rm u} + R_{\rm c} + R_{\rm b})$. Replacing $R_{\rm d}$ in equation 4 one obtains:

$$R_s = \frac{1}{\alpha_s^{\phi^0} - \alpha_d^{\phi^0}} \left[\frac{N^{\phi^0}}{N_{had}} - \alpha_d^{\phi^0} - \sum_{q \neq d,s} (\alpha_q^{\phi^0} - \alpha_d^{\phi^0}) \cdot R_q \right] \tag{11}$$

In this condition, the results obtained for the three x_p ranges are:

$$\begin{aligned} R_s &= 0.218 \pm 0.021\ (stat.)\ (x_p > 0.390) \\ R_s &= 0.229 \pm 0.022\ (stat.)\ (x_p > 0.455) \\ R_s &= 0.217 \pm 0.025\ (stat.)\ (x_p > 0.500) \end{aligned}$$

in a good agreement with those of previous item and also stable with $x_p - cut$.

3. $R_{\rm s}$ is calculated from equation (4) where the $R_{\rm q}$ ($q \neq s$) values have been taken from Standard Model (table 1). The extracted results are:

$$\begin{aligned} R_s &= 0.218 \pm 0.020\ (stat.)\ (x_p > 0.390) \\ R_s &= 0.229 \pm 0.022\ (stat.)\ (x_p > 0.455) \\ R_s &= 0.217 \pm 0.024\ (stat.)\ (x_p > 0.500) \end{aligned}$$

also in a good agreement with the results obtained in the previous items.

5.1.3 Systematic errors for ϕ^0 analysis

The following sources of systematic errors were considered :

- Systematic errors coming from the choice of the fitting functions for the signal and the background parametrization. The ability of the fitting function (signal+background) to calculate the number of ϕ^0's correctly was tested using the simulated data, where the number of ϕ^0 was known, and by smoothing the background using several ways. On top of that, after smoothing the simulated background, the combinatorial background composition was varied in simulated data by varying the production of those particles contributing significantly to the background and by fitting again the m_{KK}invariant mass distribution using the previous background smoothing. A smearing of simulated m_{KK} has also been tried to well reproduce the data m_{KK} distributions, especially for last x_p range ($x_p > 0.694$). The fit limits of the m_{KK} distribution on both data and simulation have also been varied. The obtained systematic errors ($\Delta\epsilon_{rec}$) are summarized by table 9 for each x_p range.

Table 9: *Systematic errors for the ϕ^0 number estimation.*

x_p	$\Delta\epsilon_{rec}$
$0.390 < x_p < 0.455$	4.7%
$0.455 < x_p < 0.500$	3.1%
$0.500 < x_p < 0.585$	1.6%
$0.585 < x_p < 0.694$	2.3%
$0.694 < x_p$	16.2%

The relatively high systematic error for $x_p > 0.694$ is produced by the resolution difference between data and Monte Carlo simulation mentioned in section 5.1.1. These systematic errors on the number of ϕ^0's produce an uncertainty on $R_{\rm s}$. Table 10 gives the systematic error $\Delta R_{\rm s}$ per $x_p - cut$ for each item of section 5.1.2.

Table 10: *Systematic errors on $R_{\rm s}$ due to ϕ^0 number estimation.*

$x_p - cut$	ΔN^{ϕ^0}	$\Delta R_{\rm s}$
$x_p > 0.390$	2.0%	0.007
$x_p > 0.455$	1.8%	0.006
$x_p > 0.500$	2.2%	0.006

- Errors on the measured values of $R_{\rm b}$ and $R_{\rm c}$ used in the calculation of $R_{\rm s}$. Table 11 summarize these uncertainties for items 1 and 2 of section 5.1.2. In case where $R_{\rm q}$ values are taken from Standard Model no systematic error is considered on these parameters.

Table 11: *Systematic errors $\Delta R_{\rm s}$ due errors on the measured values of $R_{\rm b}$, $R_{\rm c}$(for item 1) and $R_{\rm u}$ (for items 1',2).*

item	x_p >0.390	x_p > 0.455	x_p >0.500	x_p > 0.585	x_p >0.694
1	0.0020	0.0016	0.0013	0.0008	0.0008
1'	0.0023	0.0018	0.0015	0.0010	0.0012
2	0.0018	0.0014	0.0012	0.0007	0.0009

- Limited Monte Carlo statistics for the calculation of the $\alpha_q^{\phi^0}$ coefficients. 1.8 million simulated and reconstructed events have been used for the $\alpha_q^{\phi^0}$ evaluation producing some statistical uncertainties on these values considered as source of systematic errors for $R_{\rm s}$ evaluation (table 12).

Table 12: *Statistical errors on $\alpha_q^{\phi^0}$ coefficients as calculated from full simulation per flavour and the corresponding induced systematic errors $\Delta R_{\rm s}$ for ϕ^0 analysis.*

flavour	x_p >0.390	x_p > 0.455	x_p >0.500	x_p > 0.585	x_p >0.694
d	$3.41\text{x}10^{-5}$	$2.48\text{x}10^{-5}$	$1.88\text{x}10^{-5}$	$1.10\text{x}10^{-5}$	$4.64\text{x}10^{-6}$
u	$3.95\text{x}10^{-5}$	$2.82\text{x}10^{-5}$	$2.31\text{x}10^{-5}$	$1.58\text{x}10^{-5}$	$1.03\text{x}10^{-5}$
s	$1.55\text{x}10^{-4}$	$1.32\text{x}10^{-4}$	$1.16\text{x}10^{-4}$	$8.58\text{x}10^{-5}$	$4.69\text{x}10^{-5}$
c	$1.10\text{x}10^{-4}$	$8.42\text{x}10^{-5}$	$6.74\text{x}10^{-5}$	$3.81\text{x}10^{-5}$	$1.80\text{x}10^{-5}$
b	$5.50\text{x}10^{-5}$	$3.88\text{x}10^{-5}$	$2.85\text{x}10^{-5}$	$1.46\text{x}10^{-5}$	$3.35\text{x}10^{-6}$
$\Delta R_{\rm s}$	0.0057	0.0067	0.0071	0.0084	0.0155

- Parameters in JETSET PS 7.3. Fragmentation parameters are very important for the inclusive particle production. DELPHI collaboration has performed its own tuning of JETSET parameters [13] by using the event shape and charged particle inclusive distributions for $Z^0 \to q\bar{q}$. For the fitted parameters, a statistical and systematic error have been extracted giving the order of magnitude of the variation of these parameters to be used for the extraction of the systematic error on $R_{\rm s}$. Table 13 presents the main parameters to which $R_{\rm s}$ is sensitive, the relative variation used and the extracted $\Delta R_{\rm s}$ systematic error. From this table one can see that $\Delta R_{\rm s}$ is not very sensitive to $x_p - cut$ and that, the systematic error induced by γ_s/γ_u (probability to extract from the vacuum a $s-$quark compared to the one of extracting a $u-$ or $d-$quark) variation is by far the dominant contribution to $\Delta R_{\rm s}$.

- Branching ratios uncertainty influencing the calculation of the $\alpha_q^{\phi^0}$ coefficients. Particle decays not very well measured influencing the ϕ^0 production and momentum distribution in simulated data, modifying the $\alpha_q^{\phi^0}$ coefficients and thus, inducing a systematic error on $R_{\rm s}$were considered. For this study the main decays producing a significant variation of $R_{\rm s}$ are given by table 14. Significant reduction of $\Delta R_{\rm s}$ is observed when $x_p - cut$ increases due to the lower importance of particle decays.

Table 13: *Systematic errors from JETSET parameters variation based on generation level for ϕ^0 (the parameters have been considered to be uncorrelated).*

Parameter	Ref. Value	Variation	$\Delta R_{\rm s}$		
			$x_p > 0.390$	$x_p > 0.455$	$x_p > 0.500$
Λ_{QCD}	346 MeV	±5%	0.0017	0.0023	0.0022
Cut-off value Q_0 of Parton Shower Evolution	2.25	±20%	0.0039	0.0059	0.0078
Parameter a of Lund symmetric fragmentation function	0.50	±11%	0.0002	0.0002	0.0002
Parameter ϵ_c of Peterson fragmentation function	-0.03048	±9%	0.0008	0.0008	0.0007
Parameter ϵ_b of Peterson fragmentation function	-0.002326	±11%	0.0002	0.0002	0.0002
Suppression of s-quark pair production γ_s/γ_u	0.28	±16%	0.0213	0.0193	0.0170
Spin1(u,d)	0.50	±40%	0.0028	0.0029	0.0038
Spin1(s)	0.60	±9%	0.0002	0.0002	0.0002
$(P_{us}/P_u)/(P_s/P_d)$	0.55	±36%	0.0004	0.0019	0.0034
Total			0.0219	0.0206	0.0195

Table 14: *Systematic errors from branching ratio uncertainties for ϕ^0 analysis.*

	Branching ratio (Br)	$\Delta Br/Br$	$\Delta R_{\rm s}$		
			$x_p > 0.390$	$x_p > 0.455$	$x_p > 0.500$
1.	$Br(D_s^+ \to \phi^0\pi^+\pi^0)$	56%	0.0096	0.0065	0.0048
2.	$Br(D_s^+ \to \phi^0\pi^+)$	25%	0.0035	0.0028	0.0024
3.	$Br(\phi^0 \to K^+K^-)$	1.2%	0.0034	0.0034	0.0034
4.	$Br(D_s^+ \to \phi^0\rho^+)$	50%	0.0028	0.0015	0.0009
5.	$Br(D^0 \to \phi^0\bar{K}^0)$	12%	0.0017	0.0013	0.0010
6.	$Br(D_s^+ \to \phi^0 l\nu_l)$	25%	0.0017	0.0011	0.0008
7.	$Br(D_s^+ \to \phi^0\pi^0\pi^+\pi^0)$	50%	0.0013	0.0007	0.0004
8.	$Br(D^0 \to \phi^0\pi^0)$	50%	0.0013	0.0010	0.0008
9.	$Br(D^0 \to \phi^0\omega)$	50%	0.0008	0.0004	0.0002
10.	*Others (mainly* $B \to \phi^0 X$)		0.0045	0.0008	0.0007
	Total		0.0124	0.0083	0.0066

5.2 Charged kaon analysis

The ratio R_s was also measured using fast charged kaons identified by the Barrel Rich. In order to take into account particle identification efficiencies and contaminations for this analysis, formula 3 is expressed as:

$$R_s = \frac{1}{\alpha_s^K}\left[\frac{N^{K'}}{N_{had}}\bar{\zeta} - \sum_{q\neq s}\alpha_q^K R_q\right] \tag{12}$$

where purity $\bar{\zeta}$ is the mean kaon purity for all flavours and $N^{K'}$ the number of charged particles identified as kaons (including some other particles mainly pions identified as kaons). The averaging for the purity $\bar{\zeta}$ is explained in section 5.2.1. In this context, α_q^K is the probability to observe and identify a charged kaon originated from any $q\bar{q}$ event (from flavour q). The expected flavour composition for the selected events is given by table 15. The main contamination comes from $c\bar{c}$ events, contribution from $b\bar{b}$ events is also significant.

5.2.1 Determination of α_q^K and $K^\pm$ efficiencies and purities

To determine the coefficients α_q^K and the purities ζ_q implied in equation (12) for each flavour, a sample of 1.9 million hadronic events was used fully simulated and reconstructed with the same chain of programs as for the real data. Table 15 gives the breakdown of this sample according to the quark flavour q for the reaction $e^+e^- \rightarrow Z^0 \rightarrow q\bar{q}$ for the numbers α_q^K, ζ_q and the mean kaon reconstruction efficiency ϵ_K^{rec} (this includes also kaon identification efficiency) for the momentum range from 10 GeV/c to 20 GeV/c. No significant difference on ϵ_K^{rec} values between flavours was observed.

Table 15: *Flavour composition for the selected events and α_q^K, ζ_q and ϵ_K^{rec} parameters for charged kaon analysis.*

q	flavour fraction	α_q^K	ζ_q	ϵ_K^{rec}
d	10.5%	0.01124	0.798	21.6%
u	10.3%	0.01404	0.831	22.2%
s	39.8%	0.04294	0.953	21.1%
c	23.9%	0.03266	0.944	21.5%
b	15.5%	0.01643	0.916	23.5%

Fig. 9 shows the momentum distribution of true $K^\pm$ simulated which were found by the Barrel RICH for the various quark flavours. Fig. 10 shows the differential α_q^K values as a function of the momentum of the kaon for the various quark flavours while fig. 11 show the differential $K^\pm$ purities ζ_q. In these last two figures one can notice the relatively weak dependance of the $K^\pm$ purity on the kaon momentum and that there is no significant difference between the purities for $s-$ and $c-$quarks, and for u and d, respectively. The curve for the integral $K^\pm$ purity for all quark flavours together is found to be flat. One should also notice, however, the drop from about 95% purity for s and c, to about 80% for u and d due to different event topologies influencing the track reconstruction and particle

identification efficiency. The average $\bar{\zeta}$ was found by weighting the ζ_q values of table 15 with the number of fast kaons produced by each flavour q.

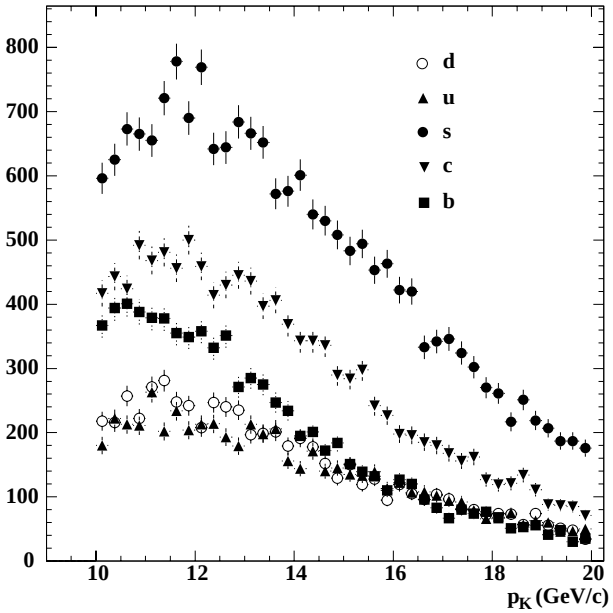

Figure 9: *Momentum distribution of charged kaons expected by DELSIM after kaon identification.*

5.2.2 R_s using charged kaons

The same assumptions have been done as for ϕ^0 analysis (section 5.1.2). The coefficients α_q^K in table 15 have been corrected for various detector effects by amounts estimated by Monte Carlo simulation. The weighted average for the purity used in equation (12) was also corrected for various detector effects. This correction was estimated by Monte Carlo simulation to be 0.53% for the purity, giving $\bar{\zeta} = 0.9062 \pm 0.0021$. Using this value, equation (12) gives the following results:

1. Assuming:

$$\begin{array}{ll} R_{\rm d} = R'_{\rm b} & \Delta R_{\rm d} = 3\Delta R_{\rm b} \\ R_{\rm u} = R_{\rm c} & \Delta R_{\rm u} = 3\Delta R_{\rm c} \end{array}$$

   where $R'_{\rm b}$ ($R_{\rm b}$ corrected for $t-$quark effect) and $R_{\rm c}$ are the experimental values, the extracted result for $R_{\rm s}$ is:

$$R_s = 0.239 \pm 0.003 \ (stat.) \tag{13}$$

2. If also OPAL value [3] and error for $R_{\rm u}$ is considered, the following result is obtained:

$$R_s = 0.244 \pm 0.003 \ (stat.) \tag{14}$$

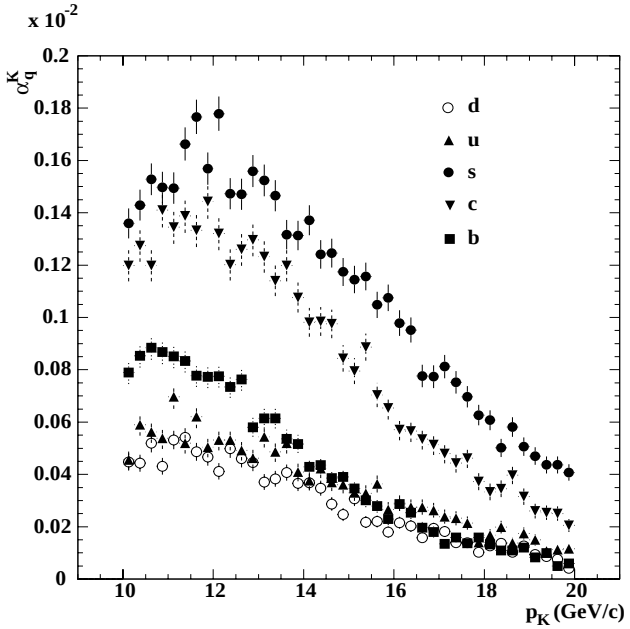

Figure 10: *Differential distribution of α_q^K for charged kaons versus momentum for the five flavours.*

3. In case where $R_{\rm b}$, $R_{\rm c}$ and $R_{\rm u}$ are the measured values and for $R_{\rm d}$ one considers that $R_{\rm d} = 1 - R_{\rm s} - (R_{\rm u} + R_{\rm c} + R_{\rm b})$, using equation 11, one can extract:

$$R_s = 0.250 \pm 0.003 \ (stat.) \tag{15}$$

4. In case where all $R_{\rm q}$ values are taken from standard model predictions, the previous results become:

$$R_s = 0.240 \pm 0.003 \ (stat.) \tag{16}$$

5.2.3 Systematic errors for charged kaon analysis

The systematic errors entering the expression 12 come from the following sources:

- Kaon efficiency and purity evaluation (due to discrepancies between simulated and real data). The systematic error $\Delta R_{\rm s}$ due to the uncertainties of the applied corrections was estimated as follows: since the uncertainties of the corrections are about of the same order of magnitude as the corrections themselves, the systematic errors induced by uncertainties on α_q^K and $\bar{\zeta}$ were taken as the absolute difference of the $R_{\rm s}$ value with both corrections in, from the $R_{\rm s}$ values where the corresponding correction was out. This gave $\Delta R_{\rm s}$=0.007 for α_q^K and $\Delta R_{\rm s}$=0.004 for $\bar{\zeta}$.

- Limited Monte Carlo statistics for α_q^K and ζ_q evaluation. The statistical errors given in table 16 for α_q^K were used as systematic errors for the same quantities in the expression 12 for $R_{\rm s}$ evaluation. Also the statistical error for the weighted

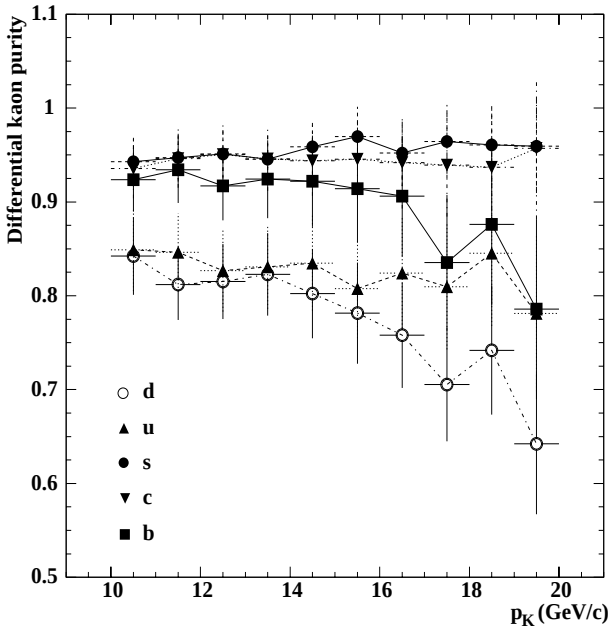

Figure 11: *Differential $K^{\pm}$ purity for all flavours.*

Table 16: *Errors on the main parameters for charged kaon analysis.*

q	$\Delta\alpha_q^K$	$\Delta\zeta_q$	$\Delta\epsilon_K^{rec}$
d	0.00017	0.015	0.34%
u	0.00021	0.016	0.36%
s	0.00033	0.010	0.17%
c	0.00032	0.013	0.23%
b	0.00020	0.015	0.31%

average $\bar{\zeta}$ was used as a systematic error. All this contributions induce a systematic error on $R_{\rm s}$ of $\Delta R_{\rm s}$=0.005 for $\alpha_{q\neq s}^K$ and $\Delta R_{\rm s}$=0.002 for α_s^K.

- Errors in the values of $R_{\rm q}$, $(q \neq s)$ used in 12. The measured errors ΔR_c and ΔR_b were taken as systematic errors for R_c and R_b. For the unmeasured R_u and R_d, the systematic errors were taken conservatively equal to $3\Delta R_c$ and $3\Delta R_b$, respectively. This gives $\Delta R_{\rm s}$=0.006, while in case where the OPAL result concerning $R_{\rm u}$ and $\Delta R_{\rm u}$ is considered, $\Delta R_{\rm s}$=0.010 is found.

- JETSET PS 7.3 parameters. The systematic errors coming from the uncertainties of various sensitive parameters of JETSET were studied by varying these values and generating new samples of Monte Carlo events from which the corresponding values of $R_{\rm s}$ were calculated. Table 17 gives a list of the parameters changed, their reference value, the variation tested and the systematic error $\Delta R_{\rm s}$ which was caused by this variation from the reference value. The total systematic error on $R_{\rm s}$ is $\Delta R_{\rm s}$=0.016.

Table 17: *Systematic errors from JETSET parameters variation based on generation level for the direct kaon study (the parameters have been considered to be uncorrelated).*

Parameter	Reference Value	Variation Tested	ΔR_s
Λ_{QCD}	346 MeV	±5%	0.0014
Cut-off value Q_0 of Parton Shower Evolution	2.25	±20%	0.0107
Parameter a of Lund symmetric fragmentation function	0.50	±11%	0.0001
Parameter ϵ_c of Peterson fragmentation function	-0.03048	±9%	0.0006
Parameter ϵ_b of Peterson fragmentation function	-0.002326	±11%	0.0002
Suppression of s-quark pair production γ_s/γ_u	0.28	±16%	0.0108
Spin1(u,d)	0.50	±40%	0.0029
Spin1(s)	0.60	±9%	0.0003
$(P_{us}/P_u)/(P_s/P_d)$	0.55	±36%	0.0019
Total			0.0157

- Branching ratios not well known. Kaon production for simulated data is affected by uncertainties on branching ratios mainly those involving B and D mesons. The main $R_{\rm s}$ uncertainties coming from this source are summarized by table 18. The biggest error is produced by $b \to K^{\pm}$. This error, $\Delta R_{\rm s}$=0.019, could be reduced if $b-$tagging technique is used to reduce the $b-$quark contamination in the selected sample.

Table 18: *Systematic errors from branching ratio uncertainties for 10 GeV/c$<$ p_K $<$ 20 GeV/c.*

	Branching ratio (Br)	$\Delta Br/Br$	ΔR_s
1.	$Br(b \to K^{\pm}X)$	21.6%	0.0162
2.	$Br(D_s^+ \to K^-X)$	$^{+108}_{-92.3}$%	0.0035
3.	$Br(D_s^+ \to K^+X)$	$^{+90}_{-70}$%	0.0027
4.	$Br(D^0 \to K^-X)$	7.4%	0.0032
5.	$Br(D^0 \to K^+X)$	$^{+17.6}_{-11.8}$%	0.0064
6.	$Br(D^+ \to K^-X)$	11.6%	0.0013
7.	$Br(D^+ \to K^+X)$	24.1%	0.0026
8.	$Others$ ($mainly$ K^{*}'s)		0.0010
	$Total$		0.0185

6 Final results and discussion

For ϕ^0 analysis, the three different ways (three items of section 5.1.2) give the same statistical errors on $R_{\rm s}$ which, for the three considered momentum ranges, are:

$$\begin{aligned} \Delta R_{\rm s}(stat.) &= 0.020 \text{ for } {\rm x_p} > 0.390 \\ &= 0.022 \text{ for } {\rm x_p} > 0.455 \\ &= 0.024 \text{ for } {\rm x_p} > 0.500 \end{aligned}$$

Moreover, one can see that the variation of the statistical error by varying $x_p - cut$ is not strong, pushing to choose the result obtained by the highest $x_p - cut$ ($x_p > 0.5$) giving the highest $s-$quark purity (77%) and thus, the lowest systematic error coming from data modeling. The systematic errors, for the different methods, are also the same (not significantly different):

$$\begin{aligned} \Delta R_{\rm s}(syst.) &= 0.027 \text{ for } {\rm x_p} > 0.390 \\ &= 0.024 \text{ for } {\rm x_p} > 0.455 \\ &= 0.023 \text{ for } {\rm x_p} > 0.500 \end{aligned}$$

One can see that, indeed, the systematic error decreases when $x_p - cut$ increases.

In order to choose the $x_p - cut$ giving the best compromise between statistical and systematic error, the total uncertainty, adding quadratically the statistical and systematic errors was calculated giving:

$$\begin{aligned} \Delta R_{\rm s}(tot.) &= 0.034 \text{ for } {\rm x_p} > 0.390 \\ &= 0.033 \text{ for } {\rm x_p} > 0.455 \\ &= 0.033 \text{ for } {\rm x_p} > 0.500 \end{aligned}$$

From these comparisons, the result obtained for $x_p > 0.5$ is chosen in order to have the highest $s-$quark purity and thus, to be less dependent on the simulation model used. Finally, the result extracted from ϕ^0 analysis is:

$$R_{\rm s} = 0.217 \pm 0.024(stat.) \pm 0.023(syst.) \tag{17}$$

where for $R_{\rm u}$ the measured value by OPAL collaboration [3] has been used.

For the charged kaon analysis, the total systematic error (including $\Delta R_{\rm u}$ from measured $R_{\rm u}$) is:

$$\Delta R_{\rm s}(syst.) = 0.028 \tag{18}$$

The statistical error is very small ($\Delta R_{\rm s}(stat.) = 0.003$) due to the large number of selected charged kaons. The final result from this analysis is:

$$R_{\rm s} = 0.244 \pm 0.003(stat.) \pm 0.028(syst.) \tag{19}$$

(where also $R_{\rm u}$ used was the measured value by OPAL collaboration) in agreement with the result extracted using fast ϕ^0's. The only negative point of this method comes from

the relatively poor $s-$quark purity which does not exceed 40%, inducing a big dependence of the result on the simulation model used. Double charged kaon tagging (one fast charged kaon in each event hemisphere) and $b-$quark tagging could help to increase the $s-$quark purity but reducing the statistics.

The two previous results being very sensitive to the JETSET strangeness suppression factor γ_s/γ_u, they have been extracted as a function of this parameter. For ϕ^0 analysis one obtains:

$$R_{\rm s}(\gamma_s/\gamma_u) = 0.706 - 2.615 \times (\gamma_s/\gamma_u) + 3.101 \times (\gamma_s/\gamma_u)^2 \tag{20}$$

while for the kaon analysis the dependence is given by:

$$R_{\rm s}(\gamma_s/\gamma_u) = 0.436 - 0.930 \times (\gamma_s/\gamma_u) + 0.870 \times (\gamma_s/\gamma_u)^2 \tag{21}$$

Combining the two results from ϕ^0 and charged kaon analysis the following result is obtained:

$$R_{\rm s} = 0.233 \pm 0.003(stat.) \pm 0.024(syst.) \tag{22}$$

The correlation between the selected events for the two methods has been neglected because only 3.7% of the selected charged kaons for the kaon analysis come from ϕ^0 decays. The systematic errors from JETSET parameters have been considered to be fully correlated between the two methods. For the combined result, the dependence between $R_{\rm s}$ and γ_s/γ_u becomes:

$$R_{\rm s}(\gamma_s/\gamma_u) = 0.549 - 1.634 \times (\gamma_s/\gamma_u) + 1.802 \times (\gamma_s/\gamma_u)^2 \tag{23}$$

The $R_{\rm s}$ value obtained by the two previous methods agree with the Standard Model value of 0.2198 and with the already measured value of $R_{\rm b}$ (0.2196 ± 0.0049) corrected for the $t-$quark effect. These results are also in agreement with $R_{d,s} = 0.230 \pm 0.010$, value already measured by OPAL collaboration [3]. Using all the measured $R_{\rm q}$ values and $\sum R_{\rm q} = 1$ one can extract $R_{\rm d}$ which has been found to be:

$$R_{\rm d} = 0.217 \pm 0.036 \tag{24}$$

7 Conclusions

Measurements of the ratio $R_{\rm s}$=$\Gamma_{\rm s\bar{s}}/\Gamma_{had}$ have been made using a sample of 1.4 million Z^0 hadronic decays using fast ϕ^0's and charged kaons to tag $\rm s\bar{s}$ events. The kaons for both methods, have been identified by the DELPHI Barrel RICH. The already measured values of $R_{\rm b}$, $R_{\rm c}$ and $R_{\rm u}$, and the Standard Model assumption that $R_d \cong R_b$ have been used. Taking into consideration $t-$quark contribution corrections which make R_b slightly smaller than R_d , it is found from the fast ϕ^0 method that:

$$R_s = 0.217 \pm 0.024(stat.) \pm 0.023(syst.)$$

with a $s-$quark purity of 77%. The major part of the systematic error comes from the JETSET parameter uncertainties. The energetic charged kaon method has given a consistent result of:

$$R_s = 0.244 \pm 0.003(stat.) \pm 0.028(syst.)$$

with a $s-$quark purity of 40%.

Combining the two previous results the following result is obtained:

$$R_s = 0.233 \pm 0.003(stat.) \pm 0.024(syst.)$$

compatible with the Standard Model prediction and the already measured R_{b} value.

References

[1] D. Bardin et al.; Zeit. Phys. **C44** (1989) 493;
Comp. Phys. Comm. 59 (1990) 303;
Nucl. Phys. **B351** (1991) 1;
Phys. Lett. **B255** (1991) 290;
D. Bardin et al. "Z–Fitter" program manual, CERN TH6443/92, May 92.

[2] LEPEWG, The LEP collaborations ALEPH, DELPHI, L3, OPAL, The LEP Electroweak Working Group and the SLD Heavy Flavour Group, 1997, *"A Combination of preliminary Electroweak Measurements and Constraints on the Standard Model"*, CERN–PPE/97–154.

[3] OPAL Collaboration, K. Ackerstaff et al., Zeit. Phys. **C76** (1997) 387.

[4] ALEPH Collaboration, D. Buskulic et al., Phys. Lett. **B313** (1993) 535.
and for example:
G.V. Borisov, *"Lifetime Tag of Events with B–hadrons with the DELPHI Detector"*, preprint IHEP (Protvino) 94–98 (1994).
DELPHI Collaboration, *"Summary of R_c measurements in DELPHI*, DELPHI 96–110 CONF 37, contributed paper to ICHEP96, Warwaw, July 1996.
OPAL Collaboration, G. Alexander et al., Zeit. Phys. **C72** (1996) 1.

[5] DELPHI Collaboration, P. Abreu et al., Zeit. Phys. **C67** (1995) 1.

[6] T. Sjöstrand, Comp. Phys. Comm. **27** (1982) 243; ibid. **28** (1983) 229;
T. Sjöstrand, "PYTHIA 5.6 and JETSET 7.3", CERN-TH.6488/92 (1992).

[7] DELPHI Collaboration, P. Abreu et al., Nucl. Instr. and Meth. **A378** (1996) 57.

[8] DELPHI Collaboration, P. Abreu et al., Zeit. Phys. **C66** (1995) 323.

[9] DELSIM User Manual, DELPHI 87–96/PROG 99, 1989;
DELSIM Reference Manual, DELPHI 87–98/PROG 100, 1989.

[10] M. Dracos, "A particle identification method for Ring Imaging Cherenkov detectors", CRN 95–21.

[11] E. Schyns, "NEWTAG–π, K, p Tagging for DELPHI RICHes", DELPHI 96–103 RICH 89 (1996).

[12] P. Pages, *"Etude de la production inclusive de mésons ϕ^0 et mesure du rapport d'embranchement du bozon Z^0 en paires de quarks étranges auprès de l'expérience DELPHI au LEP"*, PhD thesis, Université Louis Pasteur, CRN 96–19, 1996.

[13] DELPHI Collaboration, P. Abreu et al., Zeit. Phys. **C73** (1996) 11.